Calhoun

Institutional Archive of the Naval Postgraduate School

Calhoun: The NPS Institutional Archive

Faculty and Researcher Publications | Faculty and Researcher Publications

2006

Microlocal ISAR for Low Signal-to-Noise Environme

Borden, Brett

http://hdl.handle.net/10945/43814

Microlocal ISAR for Low Signal-to-Noise Environments

Brett Borden[†‡] and Margaret Cheney[†§]

Abstract— **The problem of extracting radar target information from multi-aspect high-range-resolution data is examined. We suggest a new non-imaging approach that is based on microlocal analysis, which is a mathematical theory developed to handle high-frequency asymptotics. In essence, we relate features of the target to high-frequency components of the data. To deal with realistic band-limited data, we propose an iterative algorithm (based on the generalized Radon-Hough transform) in which we estimate the high-frequency features of the data, one after another, and subtract out the corresponding band-limited components. The algorithm has been successfully tested on noisy data, and may have a number of advantages over conventional imaging methods.**

I. INTRODUCTION

HIGH range resolution (HRR) radar systems can be used to acquire range profiles which map the energy reflected from local target scatterers to the travel time of the radar pulse. Target-identification procedures based on these range profiles, however, suffer from a lack of detailed target information in dimensions orthogonal to range because all equidistant target elements are mapped to the same point. Such ambiguity can be partially removed by considering multiple pulses that interrogate the target from different directions. The different target views, which are also known as target *aspects*, collectively define a *synthetic aperture* and more complete target images can be recovered from multi-aspect data by, for example, backprojection methods [13], [14]. In inverse synthetic-aperture radar, or ISAR, this effective imaging aperture is created by the motion of the target.

Conventional image reconstruction, however, suffers from a number of shortcomings. Perhaps the most significant among these limitations is the need for phase coherence to be maintained across the entire aperture. This aperture must be large (i.e., long *slow time* duration [5]) in order to obtain good cross-range resolution. Since airborne targets will typically translate as well as rotate during the measurement interval, a pulse-to-pulse phase error may be introduced. This *range walk* problem requires that the phase error be carefully removed (*pulse range alignment*) before reconstruction can be attempted. This removal, in turn, typically requires that the target's location be extractable from the HRR data [5], [11], [19]. In the presence of noise, estimating a target's location at any instant can be problematic. Consequently, traditional ISAR imaging methods may not be applicable when the signal-to-noise or signal-to-clutter ratio is especially poor.

In addition, traditional ISAR imaging presumes a highly localized (point scatterer) model for local target structure. When this model is inappropriate—as in the case of structural dispersion—the usual images will contain artifacts. (One approach to handling non-point-like scatterers is High Definition Vector Imaging (HDVI) [1], [15].) What is more generally needed is a nontraditional *fitting* method that can be applied in data space not only to aid in the imaging of general scatterers but also to facilitate the range alignment process.

In [7] we proposed a new non-imaging approach, based on microlocal analysis, for extracting target information directly from radar data. This approach has a number of potential advantages. First, this method offers the capability of extracting target dynamics and using these dynamics to differentiate target from clutter. This separation is possible because the analysis is done in the data domain and these data are a record of range versus (slow) time, which is determined by the target dynamics. (Differentiating the target from clutter by its dynamics would be difficult or impossible in the image domain.) Second, because the approach operates in the data domain, it opens the door to the possibility of identifying targets directly from the measured data without the necessity of first constructing an image. Third, the scheme allows for artifact removal by first deleting data components not corresponding to recognizable scattering events and then forming an image from the edited data. Fourth, the microlocal theory can treat scatterers other than points, such as multiple scattering events and structural dispersion. This extension may enable us to classify scatterers in a way akin to HDVI.

Section 2 outlines the ISAR scattering model, establishes our notation, introduces some microlocal concepts, and summarizes our approach for the illustrative case of point scatterers. In section 3 we propose a method for extracting the relevant structure from the data. Finally, section 4 presents examples and results.

II. BACKGROUND

This section outlines the background material necessary for the remaining discussion. In this point-scatterer example, we exhibit the mathematical model that provides the necessary link between objects in the target domain and the data domain. This link is the foundation for the microlocal approach.

A. Model for ISAR data

We model the propagation of radar waves by the scalar wave equation (see the Appendix). We assume that the transmitting

[†] Research Department, Naval Air Warfare Center Weapons Division, China Lake, CA 93555-6100 USA

[‡] permanent address: Physics Department, Naval Postgraduate School, Monterey, CA 93943-5001

[§] permanent address: Department of Mathematical Sciences, Rensselaer Polytechnic Institute, Troy, NY 12180 USA

and receiving antennas are co-located; that the target is in the far-field of the antenna; and that the target is moving slowly enough so that it can be treated as being approximately stationary during the time interval over which the pulse sweeps across it. For simplicity we also assume that the target is supported on a plane that includes the radar. Then, in the weak-scatterer approximation, we have the following expression for the signal scattered from the n-th transmitted pulse and measured at the receiving antenna at time t:

$$s_{\rm sc}(n,t) \approx \tag{1}$$
$$\frac{1}{(4\pi R)^2} \int Q(\mathbf{z})\, \ddot{s}_{\rm inc}(t - \theta_n - 2[R + \hat{\mathbf{R}}(\theta_n) \cdot \mathbf{z}]/c)\, {\rm d}\mathbf{z}\,.$$

In this equation, R denotes the distance from the antenna to the origin of coordinates (which is fixed at the center of target rotation), $\hat{\mathbf{R}}$ denotes the unit vector from the radar to the origin, c denotes the speed of light in vacuum, $\mathbf{z} \in \mathbb{R}^2$ denotes the position on the target, $Q(\mathbf{z})$ is the target reflectivity function at the point $\mathbf{z}$, θ_n is the time at which the n-th pulse begins, and $\ddot{s}_{\rm inc}$ denotes the second derivative with respect to time of the incident field. We consider this incident field to be of the form

$$s_{\rm inc}(t) = \tag{2}$$
$$\frac{1}{\sqrt{\Delta\omega}} \int_{\omega_1}^{\omega_2} {\rm e}^{{\rm i}\omega t}\, {\rm d}\omega = \sqrt{\Delta\omega}\, {\rm e}^{{\rm i}\omega_c t}\, {\rm sinc}(t\Delta\omega/2)\,,$$

where $\Delta\omega = \omega_2 - \omega_1$ is the bandwidth and $\omega_c = (\omega_1 + \omega_2)/2$ is the center frequency. We assume the narrowband condition $\Delta\omega \ll \omega_c$. In this case, the amplitude $\sqrt{\Delta\omega}\, {\rm sinc}(t\Delta\omega/2)$ of (2) is slowly varying in comparison with the carrier modulation ${\rm e}^{{\rm i}\omega_c t}$, and this implies $\ddot{s}_{\rm inc} \approx ({\rm i}\omega_c)^2 s_{\rm inc}$.

We correlate the scattered signal with a signal of the form $s_{\rm inc}(t)$ [6] to obtain the output of the correlation receiver:

$$\eta(\theta_n, t) = \int s_{\rm sc}(n, t')\, s_{\rm inc}^*(t' - t)\, {\rm d}t' \tag{3}$$
$$= \frac{-\omega_c^2}{(4\pi R)^2} \int Q(\mathbf{z})\, \chi(t, \theta_n + 2[R + \hat{\mathbf{R}}(\theta_n) \cdot \mathbf{z}]/c)\, {\rm d}t'{\rm d}\mathbf{z}\,,$$

where the narrowband ambiguity function is here given by

$$\chi(t, \tau) = \frac{-1}{\omega_c^2} \int \ddot{s}_{\rm inc}(t' - \tau)\, s_{\rm inc}^*(t' - t)\, {\rm d}t'\,, \tag{4}$$

and where the star denotes complex conjugation.

Equation (2), when used in (4), results in

$$\chi(t, \tau) = \frac{1}{\Delta\omega} \int \int_{\omega_1}^{\omega_2} {\rm e}^{{\rm i}\omega(t'-\tau)}\, {\rm d}\omega \int_{\omega_1}^{\omega_2} {\rm e}^{-{\rm i}\omega'(t'-t)}\, {\rm d}\omega'{\rm d}t'$$
$$= \frac{1}{\Delta\omega} \int_{\omega_1}^{\omega_2} \int_{\omega_1}^{\omega_2} \delta(\omega - \omega')\, {\rm e}^{{\rm i}(-\omega\tau + {\rm i}\omega' t)}\, {\rm d}\omega'{\rm d}\omega$$
$$= \frac{1}{\Delta\omega} \int_{\omega_1}^{\omega_2} {\rm e}^{{\rm i}\omega(t-\tau)}\, {\rm d}\omega,$$
$$= {\rm e}^{{\rm i}\omega_c(t-\tau)}\, {\rm sinc}[(\Delta\omega)(t-\tau)/2]\,, \tag{5}$$

and

$$\eta(\theta_n, t) = \tag{6}$$
$$\frac{-\omega_c^2}{(4\pi R)^2 \Delta\omega} \int Q(\mathbf{z}) \int_{\omega_1}^{\omega_2} {\rm e}^{-{\rm i}\omega[t_n - 2[R+\hat{\mathbf{R}}(\theta_n)\cdot\mathbf{z}]/c]}\, {\rm d}\omega{\rm d}\mathbf{z}\,,$$

where $t_n = t - \theta_n$ is the *fast time*. We see that if $\omega_1 \to -\infty$ and $\omega_2 \to \infty$, then equation (6) is precisely a Radon transform of Q: for each θ_n, one integrates Q over the line in the $\mathbf{z}$-plane given by $t_n = 2[R + \hat{\mathbf{R}}(\theta_n) \cdot \mathbf{z}]/c$. ISAR images are traditionally produced by Radon inversion methods (such as filtered backprojection [13], [14]).

The fact that (6) is only a bandlimited version of the Radon transform results in ISAR images with limited resolution.

B. Microlocal analysis

Microlocal analysis, like the Radon-based theory, applies to the infinite-bandwidth case. In many ways, however, the infinite-bandwidth theory distills the traits relevant to target recognition from the coarser features available from limited-bandwidth data. These features are highly localized scattering centers of the target, such as corners, edges, and re-entrant structures such as ducts and engine inlets. Mathematically, such features correspond to singularities in Q.

The mathematical study of singularities is done with microlocal analysis; the term "microlocal" refers to the fact that singularities have both a location $\mathbf{x}$ and corresponding directions ξ [9].

1) Wavefront sets: Mathematically, singularities of a function such as Q is described by its *wavefront set*, which encodes both the location and direction of Q's singularities.

a) Definition: The point $(\mathbf{x}_0, \xi_0)$ is *not* in the wavefront set ${\rm WF}(f)$ of the function f if there is a smooth cutoff function ψ with $\psi(\mathbf{x}_0) \neq 0$, for which the Fourier transform $\mathcal{F}(f\psi)(\lambda\xi)$ decays rapidly (i.e., faster than any polynomial) as $\lambda \to \infty$ for ξ in a neighborhood of ξ_0.

This definition says that to determine whether $(\mathbf{x}_0, \xi_0)$ is in the wavefront set of f, one should: 1) localize around $\mathbf{x}_0$ by multiplying by a smooth function ψ supported in the neighborhood of $\mathbf{x}_0$; 2) Fourier transform $f\psi$; and 3) examine the decay of the Fourier transform in the direction ξ_0. Rapid decay of the Fourier transform in direction ξ_0 corresponds to smoothness of the function f in the direction ξ_0 [11].

b) Example. A point scatterer: If $f(\mathbf{x}) = \delta(\mathbf{x} - \mathbf{x}_0)$, then

$${\rm WF}(f) = \{(\mathbf{x}_0, \xi) : \xi \neq \mathbf{0}\}\,. \tag{7}$$

c) Example. A line: Suppose $f(\mathbf{x}) = \delta(\mathbf{x} \cdot \nu)$. Then ${\rm WF}(f) = \{(\mathbf{x}, \alpha\nu) : \mathbf{x} \cdot \nu = 0, \alpha \neq 0\}$.

Our strategy has been to work out explicitly how the wavefront set of Q corresponds to the wavefront set of η. We have done this [7] for singly and multiply scattering points and for re-entrant structures such as ducts and cavities. In the current work, we consider only the simplest case of isolated point scatterers (6), although the theory applies more generally.

2) Wavefront Set of ISAR data: In the infinite-bandwidth case, (6) is of the form of a Fourier Integral Operator (FIO) [9] applied to Q. The phase of an FIO determines how it maps wavefront sets. In particular, the mapping between wavefront sets is determined by a relation in phase space called the *canonical relation*. This relation is determined by the phase of the FIO, which in the case of point scatterers is the phase in (6):

$$\phi(\omega, \theta_n, t_n, \mathbf{z}) = \omega\left(t_n - 2[R + \hat{\mathbf{R}}(\theta_n) \cdot \mathbf{z}]/c\right)\,. \tag{8}$$

We consider only the case in which the target is rotating at a constant rate Ω and choose $\hat{\mathbf{R}}(\theta_n) \cdot \mathbf{z} = x\cos(\Omega\theta_n) + y\sin(\Omega\theta_n)$. (We have set the components of $\mathbf{z} = (x, y)$: the cross-range and down-range target coordinates, respectively.) In this case the canonical relation is

$$
\begin{aligned}
\Lambda &= \{((\theta_n, t_n; \sigma, \tau), (\mathbf{z}, \zeta)) : \mathrm{d}\phi/\mathrm{d}\omega = 0, \sigma = \mathrm{d}\phi/\mathrm{d}\theta_n, \\
&\quad \tau = \mathrm{d}\phi/\mathrm{d}t_n, \zeta = -\nabla_\mathbf{z}\phi\} \\
&= \Big\{ ((\theta_n, t_n; \sigma, \tau), (\mathbf{z}, \zeta)) : t_n = 2[R + \hat{\mathbf{R}}(\theta_n) \cdot \mathbf{z}]/c, \\
&\quad (\sigma, \tau) = \omega \left(2\Omega(x\sin(\Omega\theta_n) - y\cos(\Omega\theta_n))/c, 1\right), \\
&\quad \zeta = -2\omega(\cos(\Omega\theta_n), \sin(\Omega\theta_n))/c \Big\}.
\end{aligned}
\tag{9}
$$

The wavefront set of the radar measurements η is obtained as the set of points $(\theta_n, t_n; \sigma, \tau)$ for which there is a corresponding $(\mathbf{z}, \zeta)$ in the wavefront set of Q. In the present case, Q consists of point scatterers, so its wavefront set is a union of sets of the form (7). If we denote the location of the point scatterers by $\mathbf{z}^j = (x^j, y^j)$, then the wavefront set of η can be written

$$
\begin{aligned}
\mathrm{WF}\eta &= \bigcup_j \Big\{ (\theta_n, t_n; \sigma, \tau) : t_n = 2[R + \hat{\mathbf{R}}(\theta_n) \cdot \mathbf{z}^j]/c, \\
&\quad (\sigma, \tau) = \omega \left(2\Omega(x^j\sin(\Omega\theta_n) - y^j\cos(\Omega\theta_n))/c, 1\right) \Big\}.
\end{aligned}
\tag{10}
$$

The microlocal theory, which is based on the method of stationary phase, is a systematic way of working out high-frequency asymptotics. Strictly speaking, of course, bandlimited data are smooth and therefore the wavefront set is empty. Our analysis, however, views the bandlimited case as an approximation to the infinite-bandwidth problem.

Figure 1 shows the magnitude of data computed using equation (6) with Q consisting of three delta functions of strengths 1.0, 0.6, and 0.3 at respective positions $(-0.25, -0.25)$, $(0.3, -0.1)$, and $(0, 0.3)$. These data are roughly consistent with those obtained by scattering a pulse with center frequency of 5 GHz and 20% bandwidth from a 15-meter target. The angular aperture, i.e., the range of values of θ_n, in this example is $100°$. The sine curves predicted by (10) are clearly visible, albeit in a band-limited form.

While ISAR *imaging* schemes are usually based on equation (6), equation (10) shows that the wavefront set of the data contains considerable information about the target. This information can be extracted without forming an image. A point scatterer (whose wavefront set contains all directions ξ) located at $\mathbf{z}$ corresponds to the curve $t_n = 2[R + \hat{\mathbf{R}}(\theta_n) \cdot \mathbf{z}]/c$ in the data domain. The coordinates of this scatterer are usually estimated from the intersection of the backprojections constructed from data (i.e., lines oriented with angle $\Omega\theta_n$ and offset $2\hat{\mathbf{R}}(\theta_n) \cdot \mathbf{z}$.) But the wavefront-set analysis suggests another possibility: find the range $2\hat{\mathbf{R}}(\theta_n) \cdot \mathbf{z}$ from knowledge of t_n and estimate the cross-range position from the directions $(\sigma, \tau) = \omega \left(2\Omega(x\sin(\Omega\theta_n) - y\cos(\Omega\theta_n))/c, 1\right)$.

III. EXTRACTION OF STRUCTURE FROM THE DATA

ISAR imaging methods are usually based, one way or another, on the Radon transform and its inversion [12]. These conventional imaging methods, however, are subject to the limitations discussed in the introduction. Alternative target estimation methods are often based on parametric fitting, and one
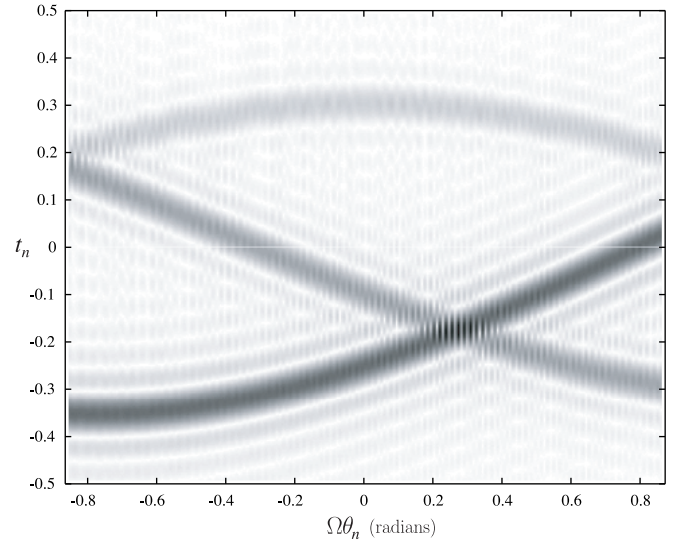

Fig. 1. This shows the magnitude of data corresponding to three point scatterers.

such scheme uses matched filters [16] (which are known to be optimal in a certain sense). Here, the appropriate matched filter approach would search for the maxima of the modulus of

$$
\mathcal{M}\{\eta\}(\mathbf{z}) = \tag{11}
$$
$$
\int \eta(\theta_n, t_n)\, \chi^*(t_n, \theta_n + 2[R + \hat{\mathbf{R}}(\theta_n) \cdot \mathbf{z}]/c)\, \mathrm{d}t_n \mathrm{d}\theta_n \,.
$$

But this approach can be computationally expensive.

Another approach is suggested by the fact that Figures 1 and 2 clearly hint at the wavefront-set structure associated with (9). The wavefront-set method presumes that we can extract the wavefront set of the data, but currently no methods are available for doing this. In the ideal case, this process would involve identifying curves in the (infinite-bandwidth) data, and the standard approach for identifying curves is to use the generalized Radon-Hough transform [10], [17]. This, by itself, is not adequate in our case because the data are band-limited. To deal with the band-limited nature of the data, we propose a modification of the CLEAN algorithm [18]—but in the data domain. In particular, we apply the generalized Radon-Hough transform to find the locus of the curve; the peak of the Radon-Hough transform tells us the most likely curve. Once we know the curve, we can determine the location of the scattering center responsible for that structure by microlocal analysis. Once we know the scattering center, we know the ambiguity structure in the data set, and can subtract that away. This process tends to eliminate the sidelobes. In summary, the algorithm is:

1) apply the generalized Radon-Hough transform to find the greatest-energy curve in the range-aspect data;
2) from this curve, use the microlocal theory to find the associated scattering center $\mathbf{z}$;
3) from the scattering center, find the associated ambiguity function $\chi_\mathbf{z}$ (the ω integral in (6));
4) subtract a (correct) multiple of this ambiguity function from the data;
5) return to step 1.

The iterations are terminated when the energy of the curve found in step 1 is less than a pre-specified threshold.

Step 4) of this algorithm is problematic because the data are highly oscillatory and small errors in the location of the scattering centers cause constructive and destructive interference in the subtraction process. Incorrect data structure subtraction can lead to further errors in following iterations. To overcome this difficulty, we use a least-squares minimization criterion to pick the multiplier μ used in subtracting the ambiguity structure from the data. In particular, we choose μ as the solution to the minimization problem

$$
\begin{aligned}
\min_{\mu} E(\mu) &= \min_{\mu} \| \eta - \mu \chi_{\mathbf{z}} \| \\
&= \min_{\mu} \sum_{\theta_n, t_n} | \eta(\theta_n, t_n) - \mu \chi_{\mathbf{z}}(\theta_n, t_n) |^2 .
\end{aligned} \tag{12}
$$

This minimization is one-dimensional and can be carried out explicitly by differentiating with respect to μ and setting the derivative equal to zero:

$$
\begin{aligned}
0 &= \frac{\mathrm{d}E}{\mathrm{d}\mu} \\
&= -2 \sum \left(\eta(\theta_n, t_n) - \mu \chi_{\mathbf{z}}(\theta_n, t_n) \right) \chi_{\mathbf{z}}^{*}(\theta_n, t_n) .
\end{aligned} \tag{13}
$$

This equation has the solution

$$
\mu = \frac{\sum \eta \chi_{\mathbf{z}}^{*}}{\sum | \chi_{\mathbf{z}} |^2} , \tag{14}
$$

and so, at each step we modify the data as

$$
\eta_{\mathrm{new}} = \eta - \mu \chi_{\mathbf{z}} . \tag{15}
$$

We note that μ is complex; its phase compensates for errors in the location of the scattering center.

IV. EXAMPLES AND RESULTS

In typical practice, the data are collected over a sufficiently narrow aperture that the curves illustrated in Figure 1 become straight lines. For simplicity, we restrict ourselves to this small-angle situation. Figure 2 shows data computed for the same three point scatterers as in Figure 1 but now corresponding to an aperture of $5°$.

Conventional Radon reconstructions [13], [14], in the small-aperture case, can be implemented by fast Fourier transform methods. The ordinary image reconstruction for the data of Figure 2 is illustrated in Figure 3.

As discussed in the previous section, we propose a wavefront-set-based scheme. For a narrow aperture, the generalized Radon-Hough transform is simply the usual Radon-Hough transform that integrates over lines:

$$
\begin{aligned}
\mathcal{H}\{\eta\}(r, \alpha) = & \\
& \int \eta(\theta_n, t_n) \delta(r - t_n \cos\alpha - \theta_n \sin\alpha) \, \mathrm{d}t_n \mathrm{d}\theta_n .
\end{aligned} \tag{16}
$$

To exercise our algorithm we apply it to the basic data of Figure 2 to which have been added varying amounts of Gaussian noise. Specifically, the data used were equal to (6) plus
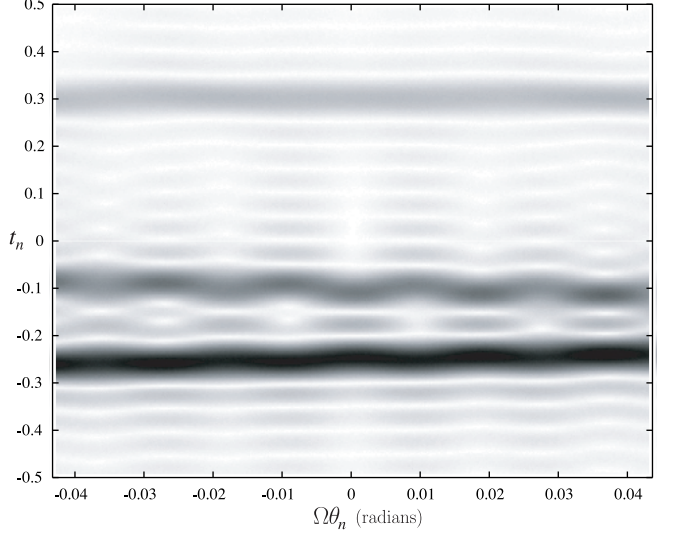

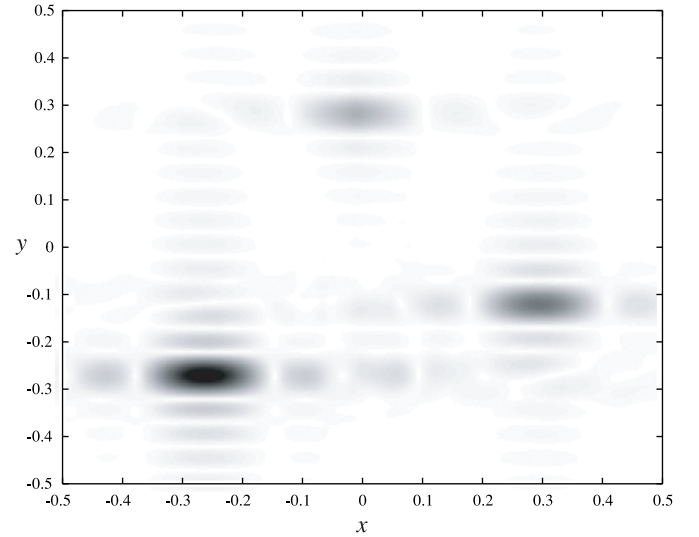Fig. 2. The data of Figure 1 restricted to the small aperture ($5°$).

Fig. 3. This shows the magnitude of a conventional reconstruction for the data of Figure 2.

$N(\theta_n, t)$ where N is a complex-valued Gaussian random variable with mean zero, standard deviation one, and amplitude A. The signal-to-noise is calculated as

$$
\mathrm{SNR} = \frac{\sum_{\theta_n, t} | \eta(\theta_n, t) |^2}{\sum_{\theta_n, t} | N(\theta_n, t) |^2} . \tag{17}
$$

Figure 4 illustrates a realization of such data for which the SNR was set to -20 dB.

To these data we applied the iterative method discussed in the previous section. The results are reported in Table I. This table lists the estimated position $\mathbf{z} = (x, y)$ of the point scatterers successively retrieved by the algorithm. The scatterer strength is given in the last row and is determined by equation (14). Successive iterations are listed from left to right.

In general, we found that the algorithm converged very rapidly, even when the signal-to-noise ratio was very poor. Observe that in the -30 dB case, the iterations terminated before
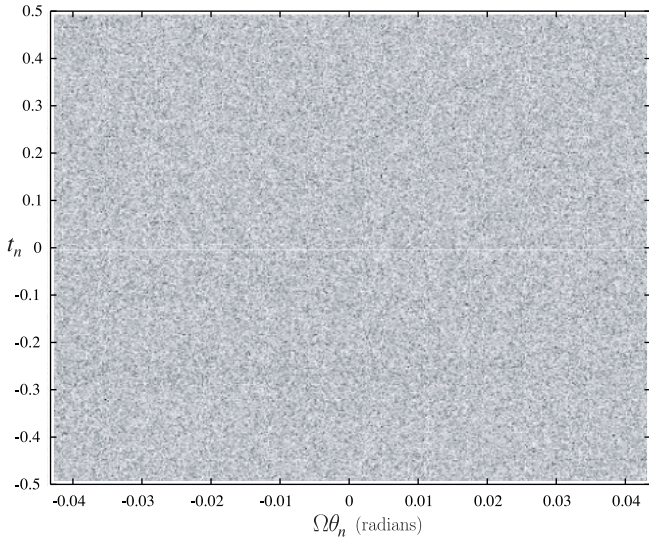
Fig. 4. Amplitude plot of noisy data of the kind used for testing the algorithm. These data were formed from those of Figure 2 plus additive (complex-valued) Gaussian noise. For this realization, SNR was set to -20 dB.

SNR	x	y	mag.
	-0.25	-0.25	1.00
True Values	0.30	-0.10	0.60
	0.00	0.30	0.30
	-0.252	-0.252	0.998
$+30$ dB	0.302	-0.101	0.599
	0.013	0.300	0.294
	-0.254	-0.256	0.987
-20 dB	0.300	-0.097	0.621
	-0.015	0.290	0.291
	-0.256	-0.245	1.005
-30 dB	0.186	-0.202	0.079
	$-$	$-$	$-$

TABLE I

(TYPICAL) ALGORITHM RESULTS USING THE DATA AS IN FIGURE 4 WITH A THRESHOLD VALUE OF 0.05. SUCCESSIVE ITERATIONS ARE LISTED FROM TOP TO BOTTOM.

the weakest scatterer could be estimated, and only the strongest scatterer was recovered correctly.

V. DISCUSSION AND CONCLUSIONS

We have suggested a new approach to ISAR target reconstruction that is appropriate to low signal-to-noise situations in which range alignment is problematic. This method is distinct from traditional imaging techniques in that it first fits a parametric curve directly to the data set, and the target characteristics are extracted directly from this curve.

This technique allows us to exploit differences, in the data domain, between the target and the noise. We have shown results of tests of the algorithm on data with additive Gaussian noise, but we have also achieved promising results using simple clutter models. This is an area of future research.

We have used the weak-scattering model here for illustration purposes only. Multiple scattering and dispersive scattering

also have well-defined wavefront sets [7] which display unique target-relevant characteristics. The foregoing analysis can be modified to account for these more general scattering situations in a straightforward way.

APPENDIX
DATA MODEL

Ultimately, the behavior of radar data is determined by scattered-field solutions to the wave equation. Since radar systems transmit and receive radio waves, we should generally examine the electromagnetic (vector) wave equation. For simplicity, however, we will examine the scalar wave equation and assume that the components of the electromagnetic field each satisfy

$$\left(\nabla^2 - c^{-2}(t, \mathbf{x})\, \partial_t^2\right) u(t, \mathbf{x}) = 0 \,. \tag{18}$$

We write the total field as a sum of the incident and scattered fields $u = u^{\mathrm{inc}} + u^{\mathrm{sc}}$; the resulting equation for u^{sc} is

$$\left(\nabla^2 - c^{-2}\, \partial_t^2\right) u^{\mathrm{sc}}(t, \mathbf{x}) = -V(t, \mathbf{x})\, \partial_t^2 u(t, \mathbf{x}) \,, \tag{19}$$

where $V(t, \mathbf{x}) = c^{-2} - c^{-2}(t, \mathbf{x})$ is the target scattering density at time t and position $\mathbf{x} \in \mathbb{R}^3$.

We can write (19) as an integral equation

$$u^{\mathrm{sc}}(t, \mathbf{x}) = \int g(t - t', \mathbf{x} - \mathbf{y}) V(t', \mathbf{y})\, \ddot{u}(t', \mathbf{y})\, \mathrm{d}t' \mathrm{d}\mathbf{y} \,, \tag{20}$$

where the dots denote partial derivatives with respect to time and [2]

$$g(t, \mathbf{x}) = \frac{\delta(t - |\mathbf{x}|/c)}{4\pi |\mathbf{x}|} \tag{21}$$

satisfies $\left(\nabla^2 - \partial_t^2\right) g(t, \mathbf{x}) = -\delta(t)\delta(\mathbf{x})$.

When the target does not appreciably perturb the incident wave, an approximation [2] called the *Born approximation* or the *single scattering approximation* is appropriate. This model replaces the full field u on the right side of (19) and (20) by the incident field u_{inc}, which converts (20) into

$$u^{\mathrm{sc}}(t, \mathbf{x}) \approx \int g(t - t', \mathbf{x} - \mathbf{y}) V(t', \mathbf{y})\, \ddot{u}^{\mathrm{inc}}(t', \mathbf{y})\, \mathrm{d}t' \mathrm{d}\mathbf{y} \,. \tag{22}$$

The value of this approximation is that it removes the nonlinearity in the inverse problem: it replaces the product of two unknowns (V and u) by a single unknown (V) multiplied by the known incident field.

We assume that the incident field is a series of pulses, beginning at times $t = \theta_n, n = 1, 2, \ldots$ from an isotropic point radiator at position $\mathbf{x}$, so that

$$u_n^{\mathrm{inc}}(t', \mathbf{y}) = \frac{s_{\mathrm{inc}}(t' - \theta_n - |\mathbf{x} - \mathbf{y}|/c)}{4\pi |\mathbf{x} - \mathbf{y}|} \,. \tag{23}$$

We also assume the start-stop approximation, i.e., we assume that the target is rotating slowly, so that for t' between θ_n and

θ_{n+1}, $V(t', \mathbf{y}) = V(\theta_n, \mathbf{y}) = Q(\mathcal{O}^{-1}(\theta_n)(\mathbf{y}))$, where $\mathcal{O}$ denotes a rotation operator (an orthogonal matrix). Here Q is the target reflectivity function. For simplicity we assume that Q is supported on a plane that includes the radar. For the more general case, see [7].

We consider the *monostatic* case, in which the transmitter and receiver are co-located. At the radar, the field due to the n-th transmitted pulse is thus $u_n^{\mathrm{sc}}(t, \mathbf{x})$. This field induces a system signal whose Born-approximated value we denote by $s_{\mathrm{sc}}(\mathbf{x}, n, t)$:

$$
\begin{aligned}
s_{\mathrm{sc}}(\mathbf{x}, n, t) &= \int \frac{\delta(t - t' - |\mathbf{x} - \mathbf{y}|/c)}{4\pi|\mathbf{x} - \mathbf{y}|} Q(\mathcal{O}^{-1}(\theta_n)(\mathbf{y})) \\
&\quad \times \frac{\ddot{s}_{\mathrm{inc}}(t' - \theta_n - |\mathbf{x} - \mathbf{y}|/c) \, \mathrm{d}t' \mathrm{d}\mathbf{y}}{4\pi|\mathbf{x} - \mathbf{y}|} \\
&= \int \frac{Q(\mathcal{O}^{-1}(\theta_n)(\mathbf{y}))}{(4\pi|\mathbf{x} - \mathbf{y}|)^2} \ddot{s}_{\mathrm{inc}}(t - \theta_n - 2|\mathbf{x} - \mathbf{y}|/c) \, \mathrm{d}\mathbf{y} \, . \quad (24)
\end{aligned}
$$

In (24), we let $t'' = t' - \theta_n$, and make the change of variables $\mathbf{z} = \mathcal{O}^{-1}(\theta_n)\mathbf{y}$. This approximation converts (24) into

$$
\begin{aligned}
s_{\mathrm{sc}}(\mathbf{x}, n, t) &= \int \frac{Q(\mathbf{z})}{(4\pi|\mathbf{x} - \mathcal{O}(\theta_n)\mathbf{z}|)^2} \\
&\quad \times \ddot{s}_{\mathrm{inc}}(t - \theta_n - 2|\mathbf{x} - \mathcal{O}(\theta_n)\mathbf{z}|/c) \, \mathrm{d}\mathbf{z} \, . \quad (25)
\end{aligned}
$$

We use the far-field approximation $|\mathbf{x} - \mathbf{w}| = |\mathbf{x}| - \hat{\mathbf{x}} \cdot \mathbf{w} + O(|\mathbf{x}|^{-1})$ (with the hat denoting unit vector) and the notation $R = |\mathbf{x}|$, $\hat{\mathbf{R}}(t) = -\mathcal{O}^{\mathrm{T}}(t)\hat{\mathbf{x}}$ to rewrite (25) as

$$
\begin{aligned}
s_{\mathrm{sc}}(\mathbf{x}, n, t) &\approx \frac{1}{(4\pi R)^2} \int Q(\mathbf{z}) \\
&\quad \times \ddot{s}_{\mathrm{inc}}(t - \theta_n - 2[R + \hat{\mathbf{R}}(\theta_n) \cdot \mathbf{z}]/c) \, \mathrm{d}\mathbf{z} \, . \quad (26)
\end{aligned}
$$

REFERENCES

[1] G.R. Benitz, "High-Defintion Vector Imaging," *Lincoln Laboratory Journal,* vol. 10, pp. 147–169, 1997.

[2] N. Bleistein, *Mathematical Methods for Wave Phenomena,* New York: Academic Press, 1984.

[3] B. Borden, *Radar Imaging of Airborne Targets: A primer for applied mathematicians and physicists,* Philadelphia: Institute of Physics, 1999.

[4] R. Brunelli and T. Poggio, "Template matching: matched spatial filters and beyond," *Pattern Recognition,* vol. 30, pp. 751–768, 1997.

[5] W.G. Carrara, R.S. Goodman, and R.M. Majewski, *Spotlight Synthetic Aperture Radar—Signal Processing Algorithms,* Boston: Artech House, 1995.

[6] C.E. Cook and M. Bernfeld, *Radar Signals: An introduction to theory and applications,* New York: Academic Press, 1967.

[7] M. Cheney and B. Borden, "The structure of radar data for range-Doppler imaging," *Inverse Problems,* in review.

[8] E.J. Candès and D.L. Donoho, "Curvelets and reconstruction of images from noisy Radon data," in *Proc. SPIE 4119: Wavelet Applications in Signal and Image Processing VIII,* A. Aldroubi, A.F. Laine, M.A. Unser eds., 2000.

[9] J.J. Duistermaat, *Fourier Integral Operators,* Boston: Birkhauser, 1996.

[10] R.O. Duda and P.E. Hart, "Use of the Hough transformation to detect lines and curves in pictures," *Comm. ACM,* vol. 15, pp. 11–15, 1972.

[11] J.C. Kirk Jr., "Motion compensation for synthetic aperture radar," *IEEE Trans. on Aerosp. Electron. Syst.,* vol. 11, pp. 338–348, 1975.

[12] D.C. Munson, D. O'Brien, and W.K. Jenkins, "A tomographic formulation of spotlight-mode synthetic aperture radar," *Proc. IEEE,* vol. 71, pp. 917, 1983.

[13] F. Natterer, *The Mathematics of Computerized Tomography,* New York: Wiley, 1986.

[14] F. Natterer and F. Wübbeling, *Mathematical Methods in Image Reconstruction,* Philadelphia: SIAM, 2001.

[15] D. Nguyen, G. Benitz, J. Kay, B. Orchard, and R. Whiting, "Superresolution HRR ATR with High Definition Vector Imaging," *IEEE Trans. on Aerosp. Electron. Syst.,* vol. 37, pp. 1267–1286, 2001.

[16] A. Papoulis, *Probability, Random Variables, and Stochastic Processes,* New York: McGraw-Hill, 1989.

[17] P.A. Toft, "Using the generalized Radon transform for detection of curves in noisy images," in *Proceedings of IEEE ICASSP 96, part IV,* pp. 2221–2225, 1996.

[18] J. Tsao and B.D. Steinberg, "Reduction of sidelobe and speckle artifacts in microwave imaging: the CLEAN technique," *IEEE Trans. Antennas Propagat.,* vol. 36, pp. 543–556, 1988.

[19] D.E. Wahl, P.H. Eichel, D.C. Ghiglia, and C.V. Jakowatz Jr.,"Phase gradient autofocus—a robust tool for high resolution SAR phase correction," *IEEE Trans. on Aerosp. Electron. Syst.,* vol. 30, pp. 827–835, 1994.